Xiayu Xu[1,2]
Xuemin Wang[1,2]
Jie Hu[1,2]
Yang Gong[1,2]
Lin Wang[3]
Wan Zhou[4]
XiuJun Li[4]
Feng Xu[1,2]*

[1]The Key Laboratory of Biomedical Information Engineering of Ministry of Education, School of Life Science and Technology, Xi'an Jiaotong University, Shaanxi, P. R. China
[2]Bioinspired Engineering & Biomechanics Center (BEBC), Xi'an Jiaotong University, Shaanxi, P. R. China
[3]College of medicine, Xi'an International University, Shaanxi, P. R. China
[4]Department of Chemistry and Biochemistry, Border Biomedical Research Center, & Biomedical Engineering (BME), University of Texas at El Paso, TX, USA

Received October 21, 2018
Revised November 18, 2018
Accepted November 20, 2018

Research Article

A smartphone-based on-site nucleic acid testing platform at point-of-care settings

We developed a smartphone-based on-site nucleic acid testing (NAT) platform that can image and analyze lateral flow nucleic acid assays at point-of-care settings. An inexpensive add-on was devised to run lateral flow assays while providing homogeneous ambient light for imaging. In addition, an Android app with a user-friendly interface was developed for the result analysis and management. Linear color calibration is implemented inside the app to minimize the colorimetric reaction difference between smartphones. A relationship function between nucleic acid concentration and colorimetric reaction was established and evaluated by leave-one-out cross validation. The predicted concentration and true concentration showed a good agreement with an R-squared value of 0.96. This smartphone-based NAT platform can be used to diagnose infectious diseases and monitor disease progression, and assess treatment efficacy, especially for resource-limited settings.

Keywords:
Lateral flow assay / Nucleic acid testing / Point-of-care diagnostics / Smartphone
DOI 10.1002/elps.201800449

1 Introduction

Nucleic acid testing (NAT) has found widespread applications in various fields, especially for the diagnosis and monitoring of infectious diseases (e.g., tuberculosis and human immunodeficiency virus (HIV) infection) that cause enormous morbidity and mortality in developing countries as reported by the World Health Organization (WHO) [1, 2]. For better management of these diseases, such as HIV infection, this NAT is required to be routinely performed and provide quantitative results [2, 3]. However, conventional NAT based on PCR is almost exclusively performed in centralized laboratories with high-end facilities by well-trained personnel [4]. Although possessing high sensitivity and specificity, this method requires complicated procedures and expensive equipment, limiting its applications in resource-limited settings. A desired form of NAT for resource-limited settings should be cost-effective, portable, easy-to-use, and disposable [2].

Researchers have made great effort to develop point-of-care (POC) NAT diagnostics. Recent advances in microfluidics and nanotechnologies provide a promising approach in reducing the cost and complexity of NAT [5], resulting in many chip- or paper-based NAT devices [6–11]. For example, Selck et al. proposed the SlipChip that could increase the robustness of amplification chemistries, especially on PCR in resource-limited settings [12]. On the other hand, lots of isothermal nucleic acid amplification technologies together with miniaturized systems have been developed, which greatly facilitate POC NAT diagnostics [13, 14]. For example, we [15] and another group [16, 17] previously reported a microfluidic platform integrated with loop-mediated isothermal amplification for detection of infectious diseases. Although these methods are able to provide cost-effective and simple tests, the resulting readout is mostly obtained either by naked eyes, which makes quantification difficult and prone-to-error, or by computer-based methods, which include capturing images using a camera, uploading the photos

Correspondence: Professor XiuJun Li, Department of Chemistry and Biochemistry, Border Biomedical Research Center, & Biomedical Engineering (BME), University of Texas at El Paso, TX, 79968, USA
E-mail: xli4@utep.edu

Abbreviations: DP, detector probe; **FDA**, Food and Drug Administration; **HIV**, human immunodeficiency virus; **LFA**, lateral flow assays; **NAT**, nucleic acid testing; **POC**, point-of-care

*Additional correspondence: Professor Feng Xu
E-mail: fengxu@xjtu.edu.cn

Color Online: See article online to view Figs. 1–5 in color.

to a computer, and colorimetric analysis using commercial software [18].

We also developed other lateral flow assays for NAT with improved sensitivity [19–21] and eventually realized paper-based sample-to-answer biosensor for NAT [22]. In these work, we utilized camera phones to record assay results and then computer for result analyses, which is not convenient especially in POC settings. To address this issue, we propose an automatic smartphone-based NAT system, which allows on-site quantification and management of the result, making it readily available for on-site diagnostics. Smartphones have shown great ability to improve accessibility and reduce costs in POC diagnostics over the past few years [23–32]. Furthermore, with high-resolution cameras and powerful processors, smartphones are able to provide high-quality images and customized image processing algorithms for accurate quantification. For example, Oncescu et al. developed a self-diagnostic tool for measuring blood cholesterol level, which is quantified by capturing and analyzing cell phone images of a standard test strip [26].

Smartphone-based attachment and even app for various lateral flow assays (colorimetric, fluorescent, and chemiluminescent) have already been reported in recent years [33–36]. However, most of the above studies are relied on off-line analyses (e.g., using ImageJ or ImagePro Plus) with the aid of a computer as well [34–36]. Lee et al. reported an Android app for image acquisition and data analysis, in which some details of the attachment and app were not given [33]. In this paper, we introduce the SmartStrip system for on-site NAT, consisting of a smartphone accessory, an Android app platform, and a disposable lateral flow assay. Integrated with the advantages of smartphone and lateral flow assay, SmartStrip is accessible, portable, and easy-to-use. In this study, using HIV-1 nucleic acid sequence as an example, the applicability of the SmartStrip system for on-site detection and analysis of NAT was demonstrated. This smartphone-based quantitative nucleic acid analysis platform can be used to diagnose infectious diseases, monitor disease progression, and assess treatment efficacy, especially for resource-limited settings.

2 Methods

2.1 Overview of the system

SmartStrip consisted of a disposable lateral flow assay, a cost-effective smartphone accessory, and a user-friendly Android app for image acquisition and analysis. The smartphone accessory was designed to hold the test strip and create uniform ambient light. Both image acquisition and colorimetric analysis were performed within the smartphone, which allows quick result quantification. The SmartStrip app was also able to store and transmit the test result, allowing further evaluation of the result in a centralized laboratory.

2.2 Fabrication of lateral flow assay

The designed test strip consisted of three parts: immersing pad, absorbent pad, and backing pad that contains the test zone and the control zone. To prevent cross-contaminations from other samples during operations, the target nucleic acid has an identical sequence chosen from long terminal repeats of HIV genome, and to recognize the target, two kinds of specific probes (detector probes (DPs) and capture probes) are used. All the oligonucleotide sequences used in this study are as follows:

DP: 5′-CACAA CAGAC GGGCA CACAC TACT-$(CH_2)_6$-HS-3’;
Capture probe: 5′-Biotin/GTCTG AGGGA TCTCT AGTTA CCAG-3′;
Control probe: 5′-AGTAG TGTGT GCCCG TCTGT TGTG/Biotin-3′;
Target nucleic acid: 5′-AGTAG TGTGT GCCCG TCTGT TG TGT GACTC TGGTA ACTAG AGATC CCTCA GAC-3′;
Control nucleic acid: 5′-GCCTC AATAA AGCTT GCCTT GA GTG CTTGT GGAAA ATCTC TAGCA GTGGC GCC-3′.

The DP is used to combine with gold nanoparticles (AuNPs) to form AuNP-DP. AuNPs with a size of 13 ± 3 nm were prepared using the reduction of chloroauric acid with trisodium citrate. Briefly, 2 OD (8.3 nmol) of DP was activated by incubation in the mixture solution of 8 μL of 500 mM acetate buffer (pH 4.76), 2 μL of 10 mM tris (2-carboxyethyl) phosphine (TCEP), and 73 μL of ultrapure water at room temperature for 1 h, and then added into 15 mL of gold nanoparticles (AuNPs, ∼4.3 nM). The mixture of AuNPs and DP was kept at 4°C for 16 h and added with a certain volume of 1% SDS to reach a final concentration of 0.01% and then of 2 M NaCl to a concentration of 150 mM, respectively. The final solution stood at 4°C for another 24 h and centrifuged at 15 000 × *g* for 25 min. The supernatant was discarded, and the red pellet was redispersed in 1 mL of buffer containing 20 mM Na3PO4, 5% BSA, 0.25% Tween 20, and 10% sucrose. The resulting solution is just AuNP-DP conjugates. Capture and control probes were biotinylated and immobilized on the nitrocellulose membrane to respectively form test and control zone via electrostatic binding via streptavidin.

The principle of the lateral flow assay is the nucleic acid hybridization reaction on the nitrocellulose membrane [19]. During an assay, the target nucleic acid, if presented, would interact with AuNP conjugates and the AuNP conjugates–target complexes would migrate along the test strip toward the absorbent pad and be captured at the test zone. The excess AuNP conjugates are captured at the control zone by probes complementary to the DPs. As a result, if the same amount of AuNP conjugates is provided in each test strip, the more AuNP conjugates captured by the test zone (darker color) and the less AuNP conjugates are left for the control zone (lighter color).

During a typical assay, a small volume (80 μL) of saline sodium citrate buffer (4×, pH 7.0) containing a designed concentration of synthesized target nucleic acids

Figure 1. Different views of SmartStrip system. (a) A front view of SmartStrip system. (b) An overview of test strip. (c) A schematic diagram of the smartphone accessory. (d) A picture of the SmartStrip system. (e) A schematic diagram of test strip carrier.

was added into a single well of a 96-well plate. Then the test strip's immersing pad was dipped into the well. The color changed as the migration of the solution, which took around 10 min to finish. After the test was done, the strip can be analyzed through the SmartStrip Android app.

2.3 The design of smartphone accessory

The hardware design is shown in Fig. 1. The smartphone accessory, weighing 29.4 g, was a self-designed phone case for an Android smartphone (Samsung GT-S5830i, 832 MHZ single core ARM Qualcomm-MSM7227 Processor, 5MP Camera with F/2.6 aperture and 3 mm focal length lens). The distance between the test strip and camera was 60 mm, which was designed to capture the entire strip with minimum white edges. The smartphone accessory can be built on other types of smartphones with a slight modification of the size of the holder. When a test strip was ready for quantification, the test strip was first put in the strip carrier, which was then inserted in the slot. To avoid the influence of ambient light, the phone case was designed to be lightproof and the flash of the smartphone was used as the light source. This compact add-on module was built on a 3D printer, with resin as printing material.

2.4 The design of SmartStrip Android app

We developed an Android app running on the smartphone (Fig. 2), which allows various types of functions, including: (i) patient account management; (ii) account security check; (iii) test instruction; (iv) new test; (v) history management; and (vi) result upload. All functions mentioned above, including the image processing algorithms, were implemented independently in the Android app. The details are described below.

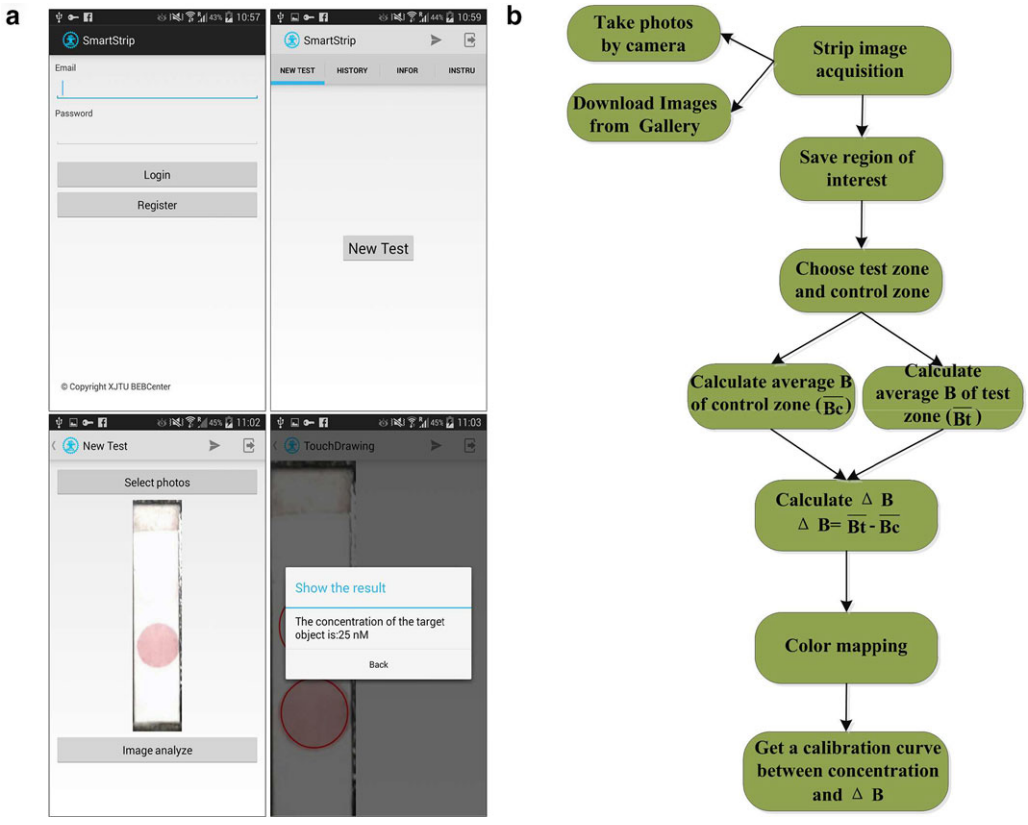

Figure 2. An overview of the SmartStrip application and its image processing algorithms. (a) Screenshots of the SmartStrip application. (b) The flow chart of colorimetric analysis algorithms.

(i) Account management and security check: SmartStrip allows multiple users on a single smartphone. Each user's data is securely stored in a personal account and protected by a password.
(ii) Test instruction: SmartStrip provides instructions for each type of test so that the users can be self-instructed before a new test.
(iii) New test: The new test function allows a user to start a new test and perform result analysis. The test image can be chosen either from the photo galleries or by taking a new photo. The result can either be stored in the smartphone or be transmitted to a doctor via email.
(iv) History management: SmartStrip allows a user to view all test records and send specific test results to his/her family doctor via email.

3 Results and discussion

3.1 Colorimetric analyses

Colorimetric assays enable visual observation and provide positive/negative results. To further evaluate disease stages and subsequently monitor disease progression and assess treatment efficacy, quantitative analyses are required. Quantitative analyses further determine the signal intensity of positive results (presence of disease), providing much more detailed information for decision-making and covering applications in both disease diagnosis and prognosis.

To build the relationship between nucleic acid concentration and colorimetric reaction, we conducted a series of lateral flow assays with different nucleic acid concentrations (i.e., 0.1, 0.5, 1, 2.5, 5, 10, 25, 50, 100, 200, 500, 1000, and 2000 nM of target nucleic acid and 100 nM of noncomplementary nucleic acid). The reported nucleic acid lateral flow assays, which are performed at room temperature, can provide adequate sensitivity as well as maintain the simplicity of the system [21]. Since the focus of this study is not the assay itself, we selected a representative assay result and performed SmartStrip-based quantitative analyses for proof of concept. However, in practical applications, the reproducibility of lateral flow assays (LFAs) may decrease due to colloidal gold batch-to-batch variations, which may require efforts from the developers and attention from the end-users.

To find the best representation of the colorimetric reaction, multiple strategies were applied. First, as explained above, the colors of the test zone and the control zone move in the opposite directions when the same amount of AuNP conjugates were provided. In conventional LFAs, the signal intensity of the control zone is independent of analyte

concentrations because there is an overdose of AuNP-DP conjugates. In our developed LFAs, the quantity of AuNP-DP is limited, and the signal intensity of the control zone as well as the detection zone was dependent on the analyte concentration. Increasing target concentration was commensurate with the development of a lower intensity band at the control zone and a higher intensity band at the detection. Hence, to enhance the colorimetric reaction differences between the test zone and the control zone, a relative colorimetric reaction (Δ) is defined as the colorimetric reaction difference between the test zone and the control zone.

$$\Delta = C_{test} - C_{control} \tag{1}$$

where C represents the colorimetric reaction. This approach offers an advantage in signal improvement as compared to the conventional operation of LFAs. Secondly, the colorimetric reaction is analyzed in three different color spaces that are widely used in literatures (i.e., RGB, HSV, and CIExyY) [23, 25, 37, 38]. The red, green, and blue channels are extracted from the original image. The hue, saturation, and value are extracted according to the following equation:

$$V = \max(R, G, B) \tag{2}$$

$$S = \begin{cases} \frac{V - \min(R,G,B)}{V} & \text{if } V \neq 0 \\ 0 & \text{otherwise} \end{cases} \tag{3}$$

$$H = \begin{cases} 60(G - B)/(V - \min(R, G, B)) & \text{if V} = \text{R} \\ 120 + 60(B - R)/(V - \min(R, G, B)) & \text{if V} = \text{G} \\ 240 + 60(R - G)/(V - \min(R, G, B)) & \text{if V} = \text{B} \end{cases} \tag{4}$$

The CIExyY values are extracted according to the following equation:

$$\begin{bmatrix} X \\ Y \\ Z \end{bmatrix} = \frac{1}{0.17697} \begin{bmatrix} 0.49 & 0.31 & 0.20 \\ 0.17697 & 0.81240 & 0.01063 \\ 0.00 & 0.01 & 0.99 \end{bmatrix} \begin{bmatrix} R \\ G \\ B \end{bmatrix} \tag{5}$$

Figure 3 shows ΔR, ΔB, and ΔV can better represent the changes in nucleic acid concentration. In this work, to keep the method simple, Δ of the blue channel (ΔB) is chosen for further analysis. Figure 3 also shows that even with these best colorimetric parameters, the correlation curve would suffer from the plateau phase when the concentration is below 2.5 nM or above 200 nM. One explanation for the plateau phase is that the color changes cannot be captured by a smartphone when the concentration is below 2.5 nM or above 200 nM. The working range of the developed SmartStrip system was 2.5–200 nM. In this study, we used synthetic single-stranded nucleic acid as our model analyte for proof of concept. For HIV detection in clinic, the target should be viral amplicons (amplified by PCR or isothermal amplification). Considering these techniques can amplify target nucleic acids across several orders of magnitude ($\sim 10^7$-fold dynamic range), the target concentration that can be detected by the SmartStrip system should be about 1.5×10^5–1.2×10^7 copies/mL prior to nucleic acid amplification, which is comparable to lots of Food and Drug Administration (FDA) approved commercial assays for monitoring HIV-1 viral load [39]. In our future work, we will use clinical samples to further explore the sensitivity and specificity of the SmartStrip system.

Although the usage of a lightproof box is able to remove much of the environmental variability in the image, the color differences caused by different smartphone hardware are inevitable (Fig. 4a), resulting in different correlation curves in colorimetric analysis. In order to calibrate the correlation curves across different smartphones, a color calibration algorithm is applied to make the correlation curve more consistent [40]. Taking the correlation curve from one smartphone (Samsung GT-S5830i) as the reference curve, the correlation curve from other smartphones was mapped to the reference curve by applying a linear transform, as shown in Fig. 4b. After color calibration, the correlation curves became more consistent so that a single relationship function can be established on the reference curve. In this way, a uniform strip appearance is achieved for different smartphone hardware.

3.2 The establishment of relationship function

A second order polynomial was fitted in the monotonic region on the reference curve (Fig. 5a) to get the best relationship function between ΔB and HIV concentration. A polynomial fitting was chosen because it is simple and easy to realize in a smartphone-based app. The precision of ΔB is 1 for an image with gray level ranging from 0 to 255.

$$\Delta B = -35.43 \log(c)^2 + 38.11 \log(c) + 65.06, \tag{6}$$

where c is the nucleic acid concentration.

To test the calibration curve, leave-one-out cross validation was used to evaluate the concentration-ΔB relationship. Leave-one-out cross validation involves using one observation as the validation set and the remaining observations as the training sample set. For example, after taking out the observation point with the concentration of 5 nM, the concentration–ΔB relationship was established using the rest observation points and this function was used to predict the concentration of the observation point that has been taken out. This was done in a recursive manner for all points. The result shows the true value and the predicted value had a high agreement with an R-square value of 0.96 (Fig. 5b).

Although the current version of SmartStrip was only tested for HIV detection, this system can be extended to the detection of multiple pathogens based on a similar NAT principle. The developed nucleic acid LFAs are dry biosensors. Detection and capture probes mainly consisted of nucleic acid sequences, which are very stable in dry status. According to a preliminary study, this assay is stable and reproducible at least in 3 months: we stored a batch of lateral flow test strips for about 3 months, and used them in LFAs in which they worked well as fresh-prepared ones. On the other hand, some commercial LFAs based on antigen–antibody reaction can be stored for 3 years. Considering nucleic acid is much more stable than protein, nucleic acid LFAs should have a

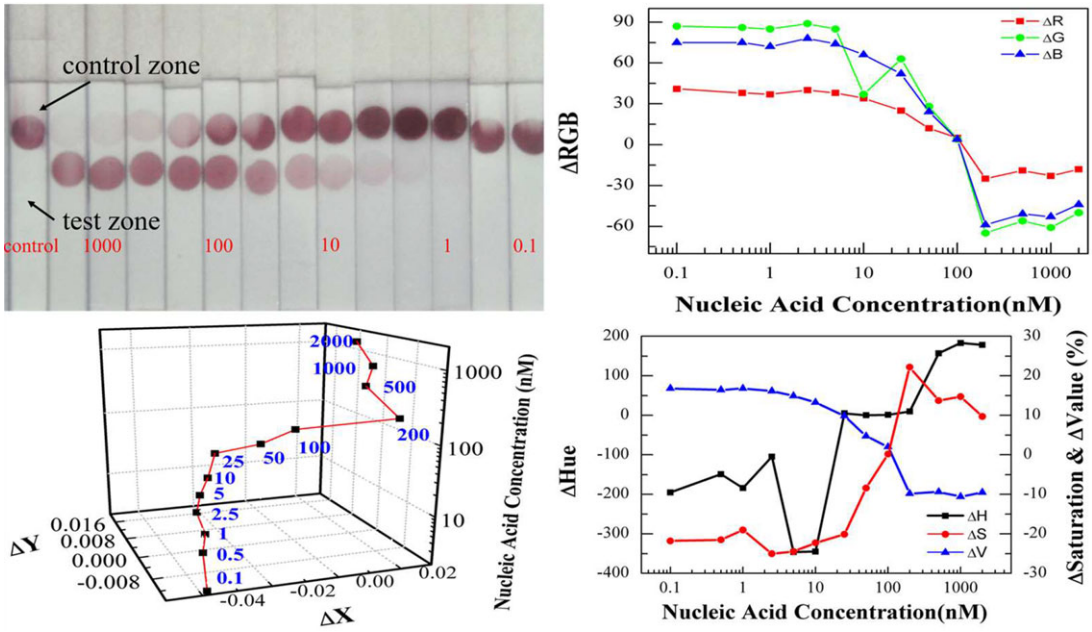

Figure 3. The selection of colorimetric reaction values. (a) Overview of the test strips used to build the correlation curve. (b) The correlation curve between nucleic acid concentration and ΔRGB. (c) The correlation curve between concentration and ΔxyY. (d) The correlation curve between nucleic acid concentration and ΔHSV.

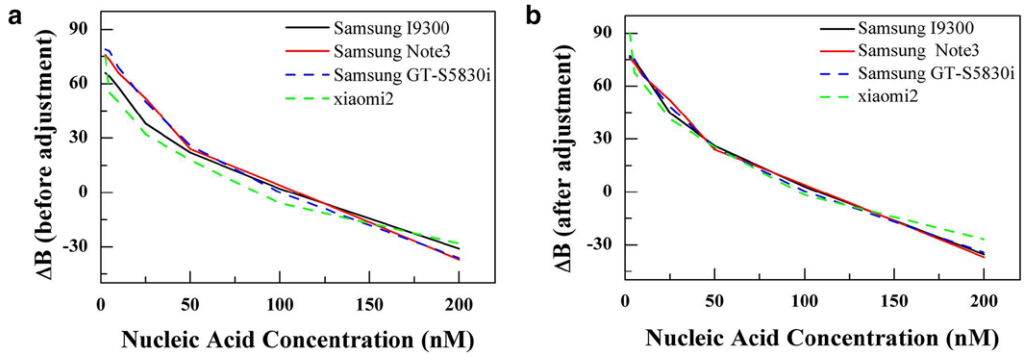

Figure 4. Color calibration among four different smartphones. (a) Colorimetric reaction curve before color calibration. (b) Colorimetric reaction curve after color calibration.

longer shelf life. However, a whole procedure of nucleic acid analysis requires sample preparation as well as detection. In this study, we report a SmartStrip system for nucleic acid detection and signal quantitative analysis at the point of care, which can be performed when the sample is ready to detect. In the meantime, we also develop a fully integrated sample-to-answer biosensor, which makes sample preparation and detection both on the paper-based substrate [41]. The Android app can also be expanded to include other nucleic acid tests. A cross-platform reproducibility is guaranteed by the hardware and software design of this system. Although the current SmartStrip was only tested for HIV detection, this system also holds the potential to extend to other test strips. New calibration relationship will need to be established. The implementation of NAT on a smartphone platform has multiple advantages. It allows on-site quantification and management of NAT with decreased cost and increased accessibility. The powerful data transmission capability of a smartphone also enables short- and long-distance communication between a remote test site and a centralized laboratory. The future work will focus on validation of the proposed system using real HIV samples.

4 Concluding remarks

We developed a SmartStrip system, a smartphone-based NAT system with low-cost accessories and automatic result quantification, which gives the system great advantages in resource-limited settings. To provide the proof-of-concept validation, we performed an HIV testing as a specific example for this system, which showed a sensitivity of 2.5 nM within 15 min and all the results were quantitatively obtained in near real time. The SmartStrip system showed great

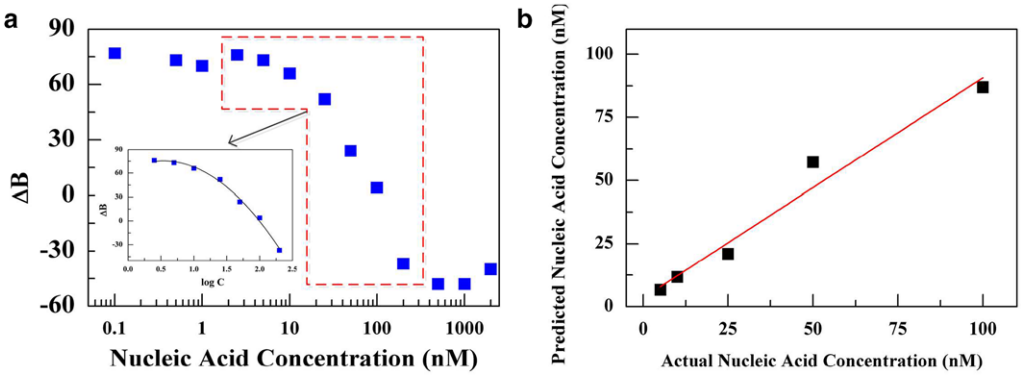

Figure 5. The establishment of relationship function and validation. (a) A calibration curve between ΔB and nucleic acid concentration. A relationship function was built in the monotonic region as indicated by the red box. (b) A comparison of the concentration between the actual value and the predicted value by SmartStrip system. The R-squared value is 0.96.

potential for the diagnosis of infectious disease in resource-limited settings.

This work was financially supported by National Natural Science Foundation of China (81401480), Shaanxi Young 1000-Talent Program and Key Program for International S&T Cooperation Projects of Shaanxi (2014KW12-01), the Key Program for Science and Technology Innovative Research Team in Shaanxi Province of China (2017KCT-22), the Program for Innovative Research Team in Yulin Shaanxi Province of China (2017KJJH-02), US NIH/NIAID (R21AI107415), and US NSF-PREM (DMR 1827745 and 1205302).

The authors have declared no conflict of interest.

5 References

[1] World Health Organization, Global Tuberculosis Report, World Health Organization, Geneva, Switzerland 2014.

[2] Wang, S., Xu, F., Demirci, U., *Biotechnol. Adv.* 2010, *28*, 770–781.

[3] Rohrman, B. A., Leautaud, V., Molyneux, E., Richards-Kortum, R. R., *PLoS One* 2012, *7*, e45611.

[4] Niemz, A., Ferguson, T. M., Boyle, D. S., *Trends Biotechnol.* 2011, *29*, 240–250.

[5] Wang, S., Inci, F., De Libero, G., Singhal, A., Demirci, U., *Biotechnol. Adv.* 2013, *31*, 438–449.

[6] Hu, J., Wang, S., Wang, L., Li, F., Pingguan-Murphy, B., Lu, T. J., Xu, F., *Biosens. Bioelectron.* 2014, *54*, 585–597.

[7] Dou, M., Dominguez, D. C., Li, X. J., Sanchez, J., Scott, G., *Anal. Chem.* 2014, *86*, 7978–7986.

[8] Zuo, P., Li, X., Dominguez, D. C., Ye, B.-C., *Lab Chip* 2013, *13*, 3921–3928.

[9] Mao, X., Ma, Y., Zhang, A., Zhang, L., Zeng, L., Liu, G., *Anal. Chem.* 2009, *81*, 1660–1668.

[10] Lie, P., Liu, J., Fang, Z., Dun, B., Zeng, L., *Chem. Commun.* 2012, *48*, 236–238.

[11] He, Y., Zhang, S., Zhang, X., Baloda, M., Gurung, A. S., Xu, H., Zhang, X., Liu, G., *Biosens. Bioelectron.* 2011, *26*, 2018–2024.

[12] Selck, D. A., Karymov, M. A., Sun, B., Ismagilov, R. F., *Anal. Chem.* 2013, *85*, 11129–11136.

[13] Craw, P., Balachandran, W., *Lab Chip* 2012, *12*, 2469–2486.

[14] Asiello, P. J., Baeumner, A. J., *Lab Chip* 2011, *11*, 1420–1430.

[15] Dou, M., Dominguez, D. C., Li, X., Sanchez, J., Scott, G., *Anal. Chem.* 2014, *86*, 7978–7986.

[16] Connelly, J. T., Rolland, J. P., Whitesides, G. M., *Anal. Chem.* 2015, *87*, 7595–7601.

[17] Rodriguez, N. M., Wong, W. S., Liu, L., Dewar, R., Klapperich, C. M., *Lab Chip* 2016, *16*, 753–763.

[18] Parolo, C., Merkoçi, A., *Chem. Soc. Rev.* 2013, *42*, 450–457.

[19] Hu, J., Wang, L., Li, F., Han, Y. L., Lin, M., Lu, T. J., Xu, F., *Lab Chip* 2013, *13*, 4352–4357.

[20] Tang, R., Yang, H., Choi, J. R., Gong, Y., Hu, J., Feng, S., Pingguan-Murphy, B., Mei, Q., Xu, F., *Talanta* 2016, *152*, 269–276.

[21] Choi, J. R., Hu, J., Feng, S., Wan Abas, W. A. B., Pingguan-Murphy, B., Xu, F., *Biosens. Bioelectron.* 2016, *79*, 98–107.

[22] Choi, J. R., Hu, J., Tang, R., Gong, Y., Feng, S., Ren, H., Wen, T., Li, X., Wan Abas, W. A. B., Pingguan-Murphy, B., Xu, F., *Lab Chip* 2016, *16*, 611–621.

[23] Shen, L., Hagen, J. A., Papautsky, I., *Lab Chip* 2012, *12*, 4240–4243.

[24] Coskun, A. F., Wong, J., Khodadadi, D., Nagi, R., Tey, A., Ozcan, A., *Lab Chip* 2013, *13*, 636–640.

[25] Oncescu, V., O'Dell, D., Erickson, D., *Lab Chip* 2013, *13*, 3232–3238.

[26] Oncescu, V., Mancuso, M., Erickson, D., *Lab Chip* 2014, *14*, 759–763.

[27] Lee, S., Oncescu, V., Mancuso, M., Mehta, S., Erickson, D., *Lab Chip* 2014, *14*, 1437–1442.

[28] Lee, D., Chou, W. P., Yeh, S.H., Chen, P. J., Chen, P. H., *Biosens. Bioelectron.* 2011, *26*, 4349–4354.

[29] Wang, S., Zhao, X., Khimji, I., Akbas, R., Qiu, W., Edwards, D., Cramer, D. W., Ye, B., Demirci, U., *Lab Chip* 2011, *11*, 3411–3418.

[30] Fronczek, C. F., Park, T. S., Harshman, D. K., Nicolini, A. M., Yoon, J.-Y., *RSC Advances* 2014, *4*, 11103–11110.

[31] Murdock, R. C., Shen, L., Griffin, D. K., Kelley-Loughnane, N., Papautsky, I., Hagen, J. A., *Anal. Chem.* 2013, *85*, 11634–11642.

[32] Wong, J. X. H., Liu, F. S. F., Yu, H.-Z., *Anal. Chem.* 2014, *86*, 11966–11971.

[33] Lee, S., Kim, G., Moon, J., *Sensors* 2013, *13*, 5109–5116.

[34] Lee, L. G., Nordman, E. S., Johnson, M. D., Oldham, M. F., *Biosensors* 2013, *3*, 360–373.

[35] Yu, L., Shi, Z., Fang, C., Zhang, Y., Liu, Y., Li, C., *Biosens. Bioelectron.* 2015, *69*, 307–315.

[36] Zangheri, M., Cevenini, L., Anfossi, L., Baggiani, C., Simoni, P., Di Nardo, F., Roda, A., *Biosens. Bioelectron.* 2015, *64*, 63–68.

[37] Hong, J. I., Chang, B.-Y., *Lab Chip* 2014, *14*, 1725–1732.

[38] Coskun, A. F., Nagi, R., Sadeghi, K., Phillips, S., Ozcan, A., *Lab Chip* 2013, *13*, 4231–4238.

[39] Dineva, M. A., Candotti, D., Fletcher-Brown, F., Allain, J.-P., Lee, H., *J. Clin. Microbiol.* 2005, *43*, 4015–4021.

[40] Bala, R., Sharma, G., Monga, V., Van de Capelle, J.-P., *IEEE Trans. Image Process.* 2005, *14*, 1172–1186.

[41] Choi, J. R., Hu, J., Tang, R., Gong, Y., Feng, S., Ren, H., Wen, T., Li, X., Wan Abas, W. A. B., Pingguan-Murphy, B., *Lab Chip* 2016, *16*, 611–621.

